

Research Paper

# *X-Ray Excited Luminescence Spectroscopy and Imaging with NaGdF<sub>4</sub>:Eu and Tb*

Meenakshi Ranasinghe<sup>1</sup>, Md. Arifuzzaman<sup>1</sup>, Apeksha C. Rajamanthrilage<sup>1</sup>, Ashley Dickey<sup>1</sup>, Joseph W. Kolis<sup>1</sup>, Mark Bolding<sup>2</sup>, Jeffrey N. Anker<sup>1,\*</sup>

<sup>1</sup> Department of Chemistry, Clemson University, Clemson, SC; and Center for Optical Materials Engineering and Technology (COMSET)

<sup>2</sup> Department of Radiology, University of Alabama at Birmingham School of Medicine, Birmingham, AL;

E-Mail: mranasi@g.clemson.edu; marifuz@g.clemson.edu; apekshr@g.clemson.edu; dickey@g.clemson.edu; kjoseph@clemson.edu; mbolding@uabmc.edu; janker@clemson.edu

\* Author to whom correspondence should be addressed; E-Mail: [janker@clemson.edu](mailto:janker@clemson.edu)

---

## **Abstract:**

X-ray excited optical luminescence from nanophosphors can be used to selectively generate light in tissue for imaging and stimulating light-responsive materials and cells. Herein, we synthesized X-ray scintillating NaGdF<sub>4</sub>: Eu and Tb nanophosphors via co-precipitate and hydrothermal methods, encapsulated with silica, functionalized with biotin, and characterized by X-ray excited optical luminescence spectroscopy and imaging. The nanophosphors synthesized by co-precipitate method were ~90 and ~106 nm in size, respectively; nanophosphors synthesized by hydrothermal method showed the highest luminescence intensity. Further, we investigated the effect of thermal annealing/calcination on the X-ray excited luminescence spectra and intensity. We observed, at high-temperature, NaGdF<sub>4</sub>: Eu@SiO<sub>2</sub> converts to NaGd<sub>9</sub>Si<sub>6</sub>O<sub>26</sub>: Eu which is also an X-ray scintillator. The particles generate light through tissue and can be selectively excited using a focused X-ray source for imaging and light generation applications. The particles also act as MRI contrast agents for multi-modal localization.

**Keywords:** Nanophosphors, XEOL, Imaging

---

## **1. Introduction**

Light can be a powerful tool for studying biochemistry in cells and tissue and for stimulating responses from genetically engineered light-sensitive neurons (optogenetics) or photo-released drugs. The challenge for delivering or retrieving light from deep tissue is that scattering in the tissue prevents light from travelling ballistically, and the point spread function is typically >1 cm through 1 cm of tissue, also the light is attenuated by the tissue [1,2]. One approach that circumvents these problems is to use X-rays to pass through the tissue with far less scattering, and generate visible light locally after

absorption by scintillators in the tissue. Scintillators are luminescent materials that absorb high-energy radiation ( $\gamma$ - and X-ray photons, high energy ions, neutrons, or other subatomic particles) and emit UV, visible and/or NIR light [1,2]. These materials are widely used radiation detection [3] and imaging applications [4–6], and occasionally in external power-free light generation applications (e.g., old luminescent watches, emergency lighting and gun sites) [7]. Recently, there has been much interest in developing scintillator nanophosphors for improved X-ray luminescence imaging [8–10], radiation imaging [9,11,12], and as a potential light source for photochemistry and photobiology (e.g., X-ray excited optogenetics [13]).

Rare-earth doped materials (NaGdF<sub>4</sub>: Eu [14,15] and Tb [16], GdO<sub>2</sub>S<sub>2</sub>: Eu and Tb [10], YAG: Nd, LuAG: Tm, Lu<sub>2</sub>SiO<sub>5</sub>: Ce [17]) have interesting properties such as narrow and distinct spectral emission peaks, long optical penetration depth, negligible autofluorescence background, photochemical stability and low toxicity [6]. Among them, rare-earth fluorides (NaGdF<sub>4</sub>: Eu and Tb) are been considered as excellent down-conversion luminescent host matrices. They usually have high refractive indices and low phonon energies, which cause a low probability of nonradiative decay and higher luminescent quantum yields compared to oxide hosts and other inorganic matrices [18].

In this paper, we synthesized Eu and Tb doped NaGdF<sub>4</sub> (NaGdF<sub>4</sub>: Eu and NaGdF<sub>4</sub>: Tb) nanoparticles and showed that they could be selectively excited in solution using a focused X-ray source. We discuss how changes in synthesis methods and functionalization affect the luminescence intensity. We also show that the particles serve as T1 and T2 MRI contrast agents which would be useful for multi-modal imaging applications.

## 2. Results and Discussion

We synthesized NaGdF<sub>4</sub>:Eu and NaGdF<sub>4</sub>:Tb nanophosphors via co-precipitation and hydrothermal methods and studied the effect of dopant concentration on their optical spectra and crystal diffraction patterns. Next we encapsulated in silica to prevent thermal sintering and studied the effect of thermal treatment; we functionalized the nanophosphors with biotin and showed that we could excite colloidal suspensions of particles with a focused X-ray beam and image the luminescence through tissue; finally, we explored the possibility of multimodal imaging based on spectrally distinct features of the nanophosphors as well as MRI contrast.

### 2.1 Synthesizing NaGdF<sub>4</sub>: Eu and NaGdF<sub>4</sub>: Tb nanoparticles:

In the NaGdF<sub>4</sub> nanophosphor synthesis, citrate acts as a complexing and dispersing agent that forms a La<sup>3+</sup>-Cit<sup>3-</sup> complex and disperse in DI water. Upon addition of excess NaF, La<sup>3+</sup> released from the complex reacts with Na<sup>+</sup> and F<sup>-</sup> to form NaGdF<sub>4</sub> nuclei. After the formation of NaGdF<sub>4</sub>: Eu and Tb, the citrate serves as a surfactant which controls nanoparticle growth and prevents aggregation [15,19].

#### 2.1.1 Co-precipitate method

The co-precipitate synthesis process is presented in Figure 1A. The nanoparticles synthesized using the co-precipitate method at room temperature were approximately spherical in shape (Figures 1B1 and 1C1). The Eu-doped and Tb-doped nanophosphors respective had average diameters of  $\sim 90$  nm (Figure 1A2) and 106 nm (Figure 1C2). The XRD diffraction peaks displayed the presence of hexagonal ( $\beta$ -phase)  $\text{NaGdF}_4$  (Figure 1B3 and 1C3) indexed to the standard data (JCPDS 00-027-0699), with relatively large peak widths indicating small crystal domain sizes ( $\sim 55$  Å  $\text{NaGdF}_4$ : Eu and  $\sim 59$  Å  $\text{NaGdF}_4$ : Tb according to the Scherrer equation).

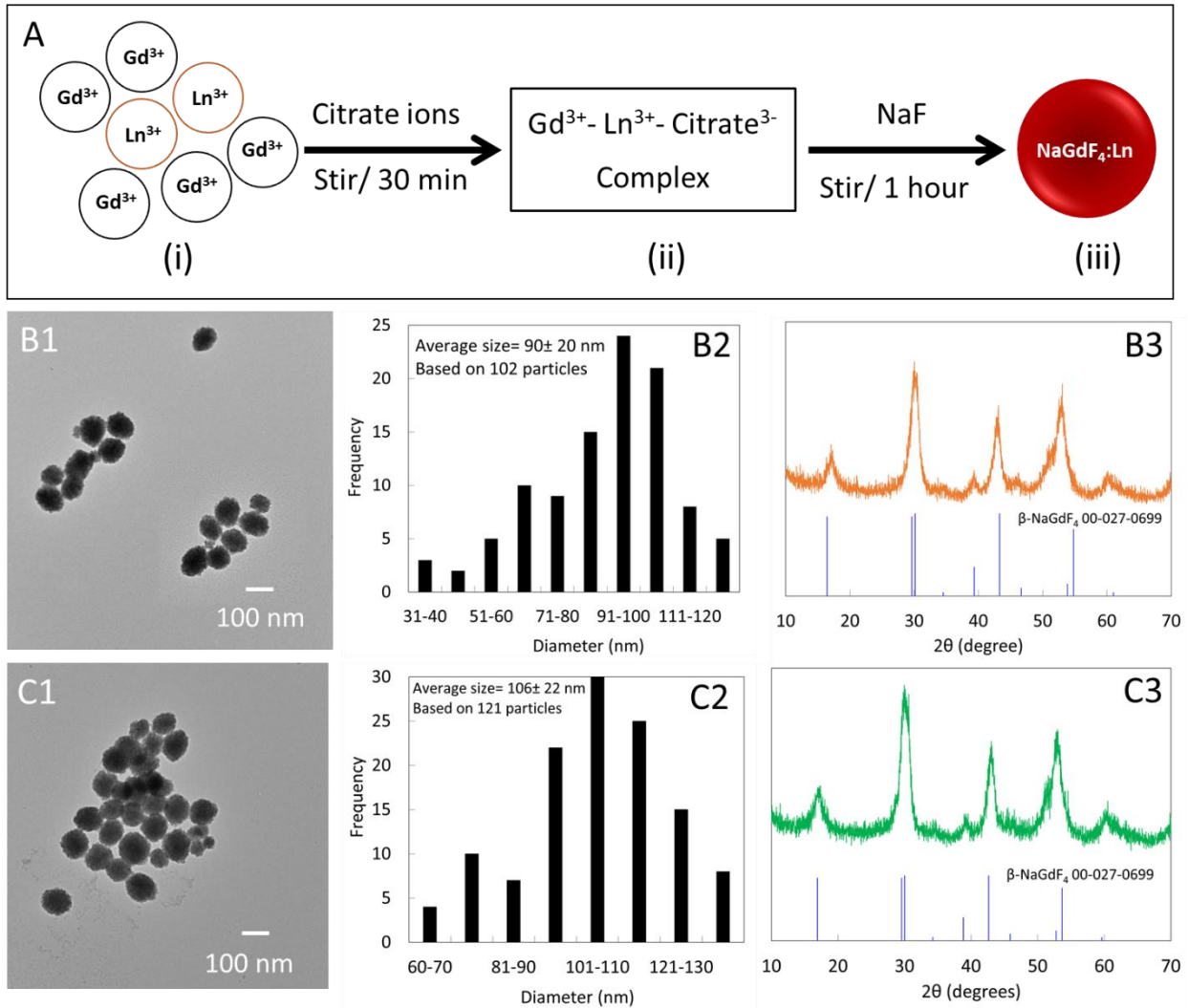


**Figure 1.** (A) Schematic illustration of nanoparticles synthesis according to co-precipitate method. (i) Mixture of  $\text{Gd}(\text{NO}_3)_3$  and  $\text{Eu}(\text{NO}_3)_3$  or  $\text{Tb}(\text{NO}_3)_3$ , (ii)  $\text{Ln}^{3+}$ -Citrate $^{3-}$  complex appears as a clear solution, (iii) Formation of  $\text{NaGdF}_4:\text{Ln}^{3+}$  nanoparticles. TEM images of (B1)  $\text{NaGdF}_4:\text{Eu}$  and (C1)  $\text{NaGdF}_4:\text{Tb}$  nanophosphors. Histograms of the average diameter of (B2)  $\text{NaGdF}_4:\text{Eu}$  and (C2)  $\text{NaGdF}_4:\text{Tb}$ . Powder XRD pattern compared to PDF cards 27-0699 of (B3)  $\text{NaGdF}_4:\text{Eu}$  and (C3)  $\text{NaGdF}_4:\text{Tb}$ .

The optical properties of rare-earth doped nanoparticles are determined by the chemical properties of doping ions and matrix. Figure 2 shows the X-ray excited optical luminescence spectrum of  $\text{NaGdF}_4:\text{Eu}$ . There are three characteristic peaks in the visible range of the electromagnetic spectrum, at around 589 nm, 615 nm and 691 nm that corresponding to  $^5\text{D}_0 \rightarrow ^7\text{F}_1$ ,  $^5\text{D}_0 \rightarrow ^7\text{F}_2$ ,  $^5\text{D}_0 \rightarrow ^7\text{F}_4$  transitions

[10,14]. Tb doped NaGdF<sub>4</sub> has four characteristic peaks in the visible range, at around 489 nm, 543 nm, 585 nm and 620 nm that corresponding to <sup>5</sup>D<sub>4</sub>→<sup>7</sup>F<sub>6</sub>, <sup>5</sup>D<sub>4</sub>→<sup>7</sup>F<sub>5</sub>, <sup>5</sup>D<sub>4</sub>→<sup>7</sup>F<sub>4</sub>, <sup>5</sup>D<sub>4</sub>→<sup>7</sup>F<sub>3</sub> transitions [10,20]. Since the luminescence intensity depends upon dopant concentration, we varied the amount of Eu and Tb compared to Gd<sup>3+</sup> in the reaction mixture. Figures 2A and 2B show the luminescence spectra for Eu- and Tb-doped nanophosphors, respectively. The dopant:Gd molar concentrations in the NaGdF<sub>4</sub> synthesis reaction were 0.1% (bottom), 1%, 15%, 20% and 100% (top). A base value has been added to each spectrum to avoid spectral overlapping. At low and high molar ratios of both Eu and Tb doped NaGdF<sub>4</sub> nanoparticles showed low luminescence intensity due to lack of luminescence centers and self-quenching, respectively. Intermediate concentrations, 1%, 15% and 20% in Eu-doped NaGdF<sub>4</sub> showed the highest although similar luminescence intensities and in Tb-doped NaGdF<sub>4</sub> 20% showed the highest intensity.

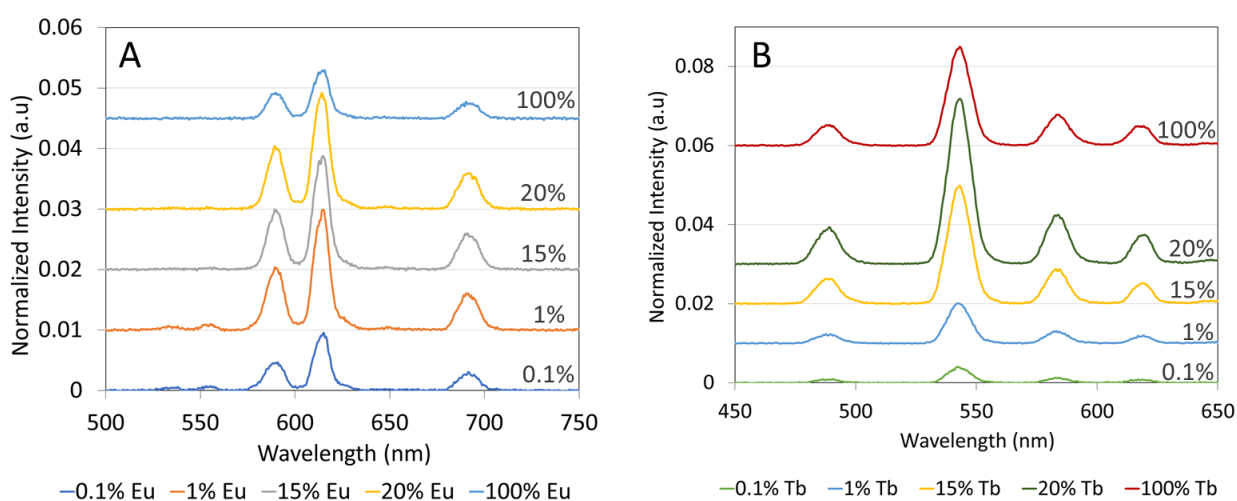


**Figure 2.** X-ray excited optical luminescence (XEOL) of (A) NaGdF<sub>4</sub>:Eu and (B) NaGdF<sub>4</sub>:Tb nanophosphors. Eu and Tb dopant fraction (mol% added to reagents vs Gd) of NaGdF<sub>4</sub> nanoparticles varied from 0.1% to 100%. X-ray luminescence intensities of nanoparticles were normalized to the height of 620 nm peak of commercial GOS:Eu and Tb microphosphors. Spectra have been vertically displaced for ease of comparison.

### 2.1.2 Hydrothermal method

The Hydrothermal synthesis process is presented in Figure 3A. The crystallinity of inorganic crystals plays an important role in X-ray luminescence intensity where large crystal domain size results in high luminescence intensity [10]. During the hydrothermal process, nanoparticles recrystallize to rearrange the crystal structure. The nanoparticles synthesized using the co-precipitate method at room temperature were hydrothermally treated to increase the crystallinity and thereby, enhance the X-ray luminescence intensity. The hydrothermally treated nanophosphors were irregularly shaped (Figures 3B1 and 3B2), however, narrow peaks in the powder XRD pattern (Figure 3B3) confirmed the increased crystallinity compared to nanoparticles synthesized at room temperature.

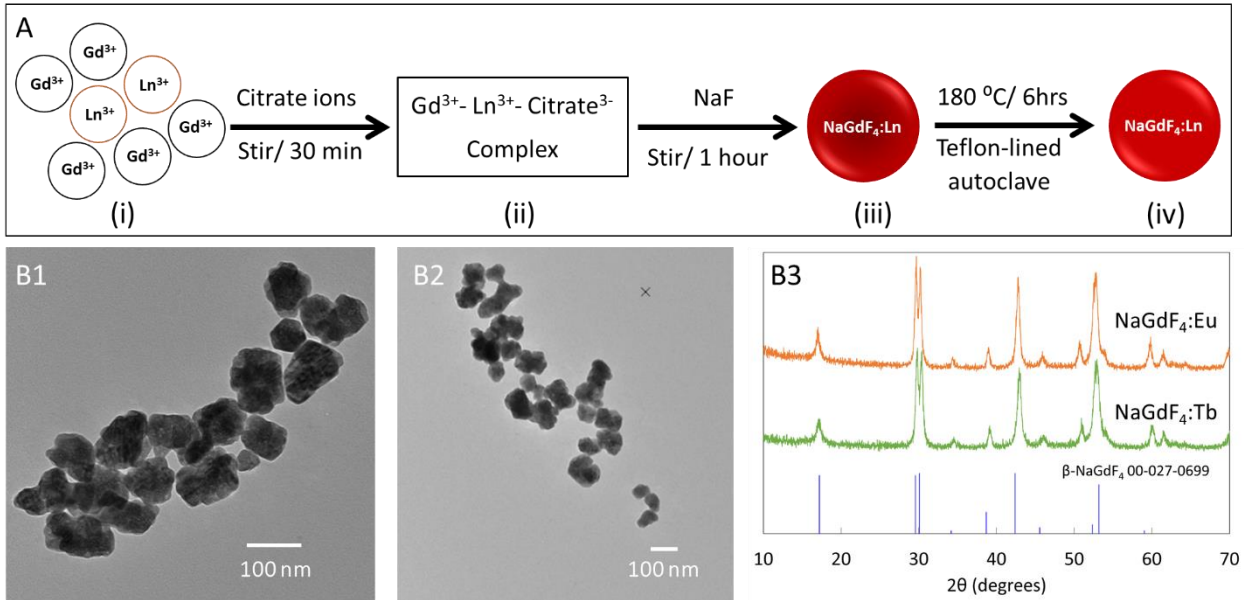


**Figure 3.** (A) Schematic illustration of nanoparticles synthesis according to co-precipitate method. (i) Mixture of  $\text{Gd}(\text{NO}_3)_3$  and  $\text{Eu}(\text{NO}_3)_3$  or  $\text{Tb}(\text{NO}_3)_3$ , (ii)  $\text{Ln}^{3+}$ -Citrate $^{3-}$  complex appears as a clear solution, (iii) Formation of  $\text{NaGdF}_4:\text{Ln}^{3+}$  nanoparticles, (iv) Hydrothermally treated  $\text{NaGdF}_4:\text{Ln}^{3+}$  nanoparticles. TEM images of hydrothermally treated (B1)  $\text{NaGdF}_4:\text{Eu}$  and (B2)  $\text{NaGdF}_4:\text{Tb}$  nanophosphors. (B3) Powder XRD pattern compared to PDF cards 27-0699 of  $\text{NaGdF}_4:\text{Eu}$  and  $\text{NaGdF}_4:\text{Tb}$ .

Hydrothermally treated nanoparticles showed enhanced X-ray luminescence intensity by a factor of 2-2.5 compared to nanoparticles synthesized at room temperature. 15% Eu doped  $\text{NaGdF}_4$  showed the highest intensity however, 1% and 20% Eu doped  $\text{NaGdF}_4$  showed high values close to the highest intensity (Figure 4A). The X-ray luminescence intensity of 15% Tb doped  $\text{NaGdF}_4$  had the highest intensity and 20% Tb doped  $\text{NaGdF}_4$  showed an intensity close to the highest value (Figure 4B).

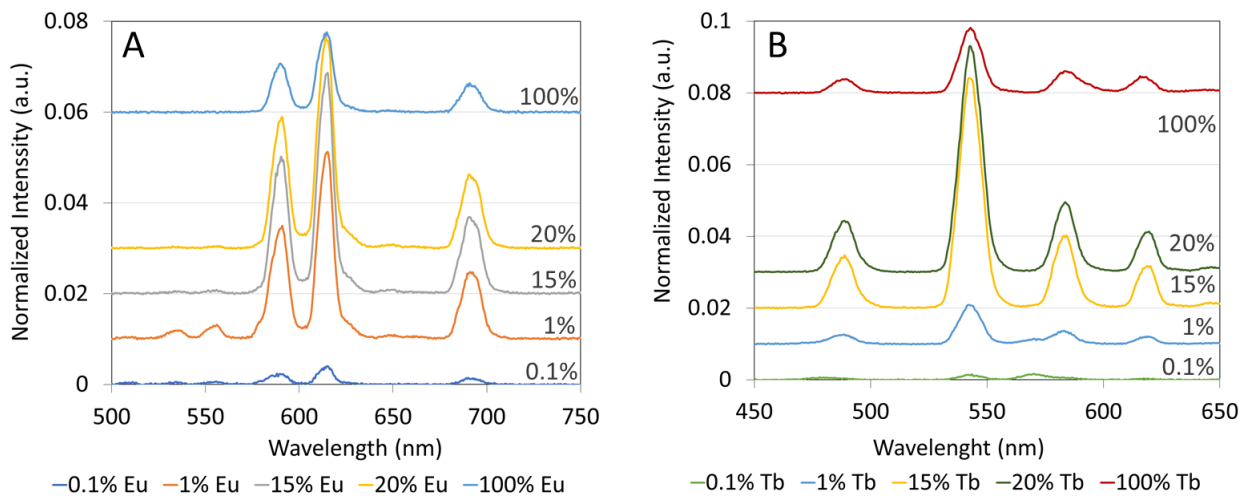


**Figure 4.** XEO of hydrothermally treated (A)  $\text{NaGdF}_4:\text{Eu}$  and (B)  $\text{NaGdF}_4:\text{Tb}$  nanophosphor. Mol fraction of Eu and Tb dopant vs. Gd in reagent mixture varied from 0.1% to 100%. X-ray luminescence intensities of nanoparticles were normalized to the height of 620 nm peak of commercial GOS: Eu and Tb microparticles. Spectra have been vertically displaced by adding a baseline for ease of comparison.

## 2.2 Silica-coated $\text{NaGdF}_4$ : Eu and Tb nanoparticles

NaGdF<sub>4</sub>:Eu nanophosphors, synthesized at room temperature, were coated with silica before further experiments. The silica can protect nanophosphors from aggregation and facilitate functionalization for biological applications. Figure 5A presents the NaGdF<sub>4</sub> silica coating process. In electron microscopy images (Figure 5B1) the silica coating appeared as a ~15 nm thick shell around the nanoparticles. The average diameter of NaGdF<sub>4</sub>:Eu@SiO<sub>2</sub> nanoparticles was about 120 nm (Figure 5B2).

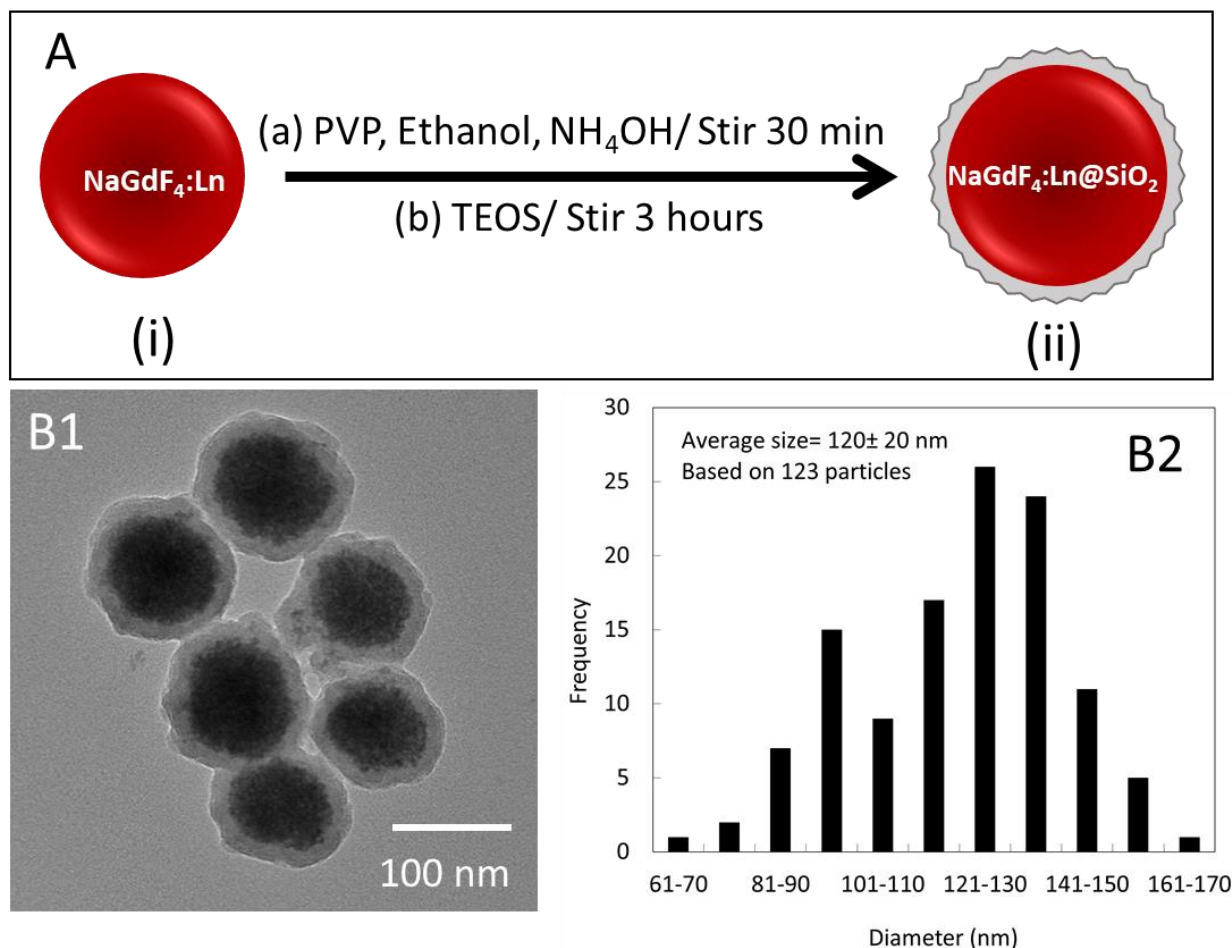


**Figure 5.** (A) Schematic illustration of nanoparticle coating with silica. (i) NaGdF<sub>4</sub>:Ln<sup>3+</sup> nanoparticles, (ii) Silica-coated NaGdF<sub>4</sub>:Ln<sup>3+</sup> nanoparticles. (B1) TEM images of silica-coated NaGdF<sub>4</sub> nanophosphors Eu-doped. (B2) Histograms of the diameter of silica-coated NaGdF<sub>4</sub>:Eu.

Both Tb-doped and Eu-doped nanophosphors showed reduced X-ray luminescence after coating with silica for the same mass of material. After coating, the NaGdF<sub>4</sub>:Eu nanophosphors reduced intensity by ~42% (Figure 6A). This is largely explained by the additional silica which increased the mass by 65% (based on particle diameter, coating thickness, and density of NaGdF<sub>4</sub> core and silica shell), while not providing any additional luminescent material.

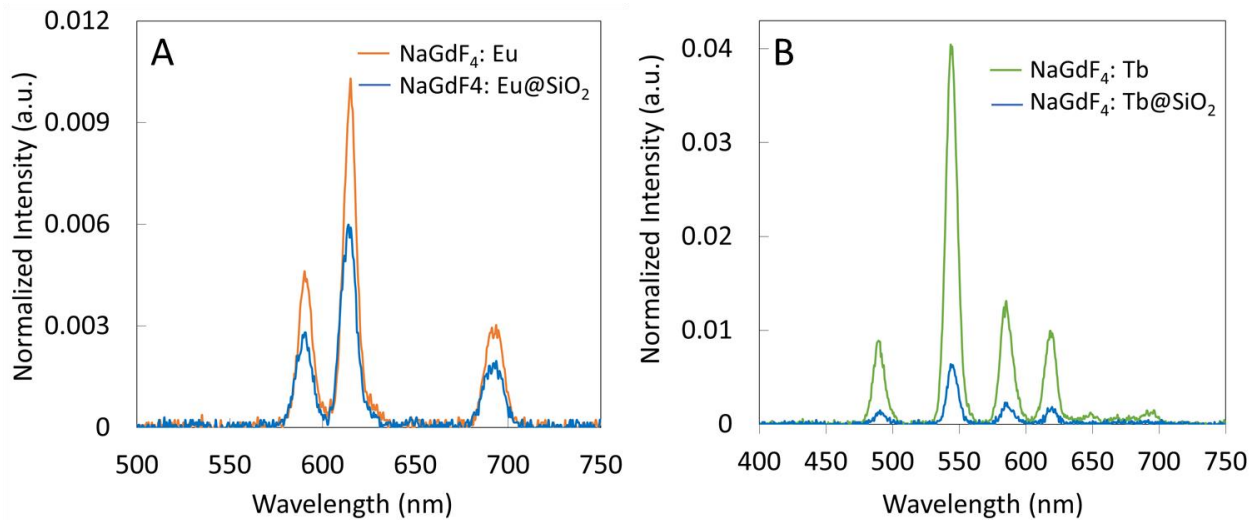


**Figure 6.** XEOL spectra of silica-coated (A) NaGdF<sub>4</sub>:Eu and (B) NaGdF<sub>4</sub>:Tb compared to NaGdF<sub>4</sub>:Eu and NaGdF<sub>4</sub>:Tb synthesized using co-precipitate method.

### 2.3 Annealing NaGdF<sub>4</sub>: Eu nanoparticles

Nanoparticles synthesized using the co-precipitate method and coated with silica have low luminescence intensity which minimizes most *in vivo* applications such as deep tissue imaging and implantable biosensors. High temperature annealing could enhance its luminescence by removing crystal defects, increasing crystal domain size and removing trapped water and carbon dioxide [21,22]. Unfortunately, when we annealed our nanophosphors at temperatures above 700 °C, we found that the particle aggregated. For example, Figure 7A shows that after thermal annealing at 1000 °C, the NaGdF<sub>4</sub>:Eu nanophosphors aggregated and fused making a structure too large for many biological applications. However, its luminescence intensity was increased by a factor of ~7 compared to nanoparticles synthesized by the co-precipitate method.

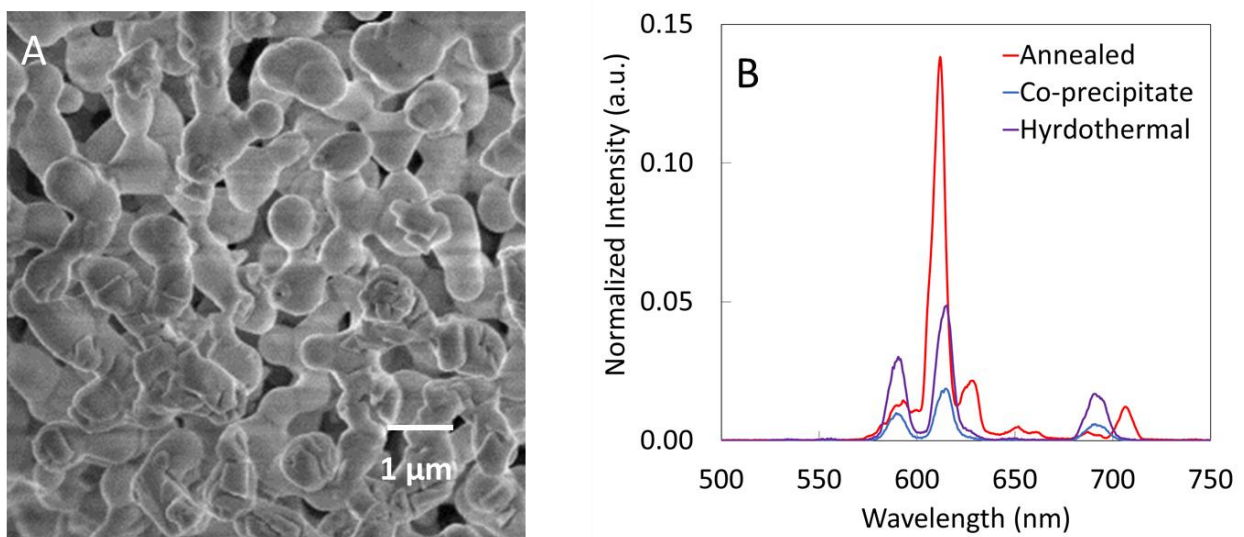


**Figure 7.** (A) SEM image and (B) XEOL of NaGdF<sub>4</sub>:Eu annealed at 1000 °C for 6 hrs compared to NaGdF<sub>4</sub>:Eu nanoparticles synthesized using co-precipitate and hydrothermal methods.

Silica coating can act as a protective layer, preventing particles from aggregating and fusing during the annealing process[21]. Annealed nanoparticles at 400 °C (Figure 8A) showed separate particles with a thin silica coating. Annealing at 600 °C (Figure 8B) showed single and separate nanoparticles with a silica shell, and nanophosphor core, but the core compressed, and some void space was apparent. Annealing at 1000 °C (Figure 8C) caused the nanoparticles to aggregate, although not to the extent of forming the large porous structures observed without coating (Figure 7C).

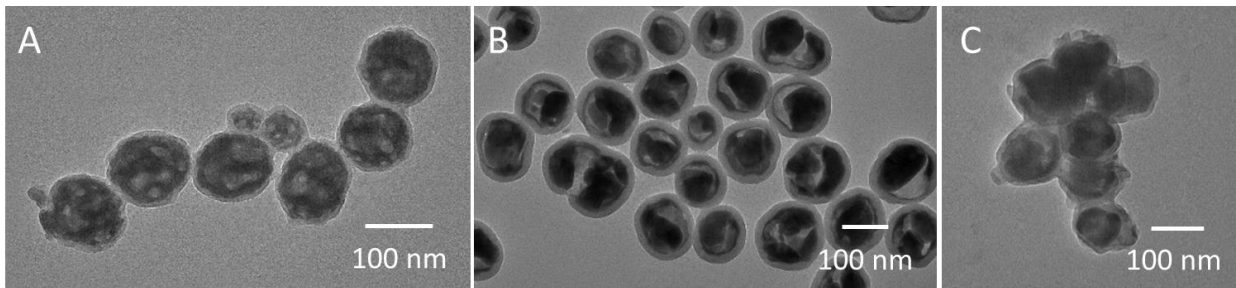


**Figure 8.** TEM images of NaGdF<sub>4</sub>:Eu@SiO<sub>2</sub> nanoparticles annealed at (A) 400 °C, (B) 600 °C (C) 1000 °C.

Annealing at 400 °C and 600 °C increased the luminescence intensity by a factor of  $\sim 1.5$  and  $\sim 3$  compared to silica-coated nanoparticles. Among the three annealing temperatures, 1000 °C showed the lowest intensity (Figure 9A). We also observed that XEOL spectrum red-shifted at high temperature (600 °C and 1000 °C). This spectral shift could potentially be useful for generating nanophosphors with distinguishable spectra for multi-modal imaging, and likely arises from changes in composition and crystal field. Indeed, powder XRD data confirmed the formation of sodium gadolinium silicate compound by reacting with the silica layer: XRD spectra display the presence of NaGd<sub>9</sub>Si<sub>6</sub>O<sub>26</sub>:Eu (Figure 9B) indexed to the standard data (JCPDS 00-056-0184). Additionally, we observe that the 600 °C annealed samples have sharper peaks indicating larger crystal domains, which likely reduces quenching from the surface and defects[10]. On balance, the 600 °C annealing appeared to give the best performance, albeit with a spectral shift.

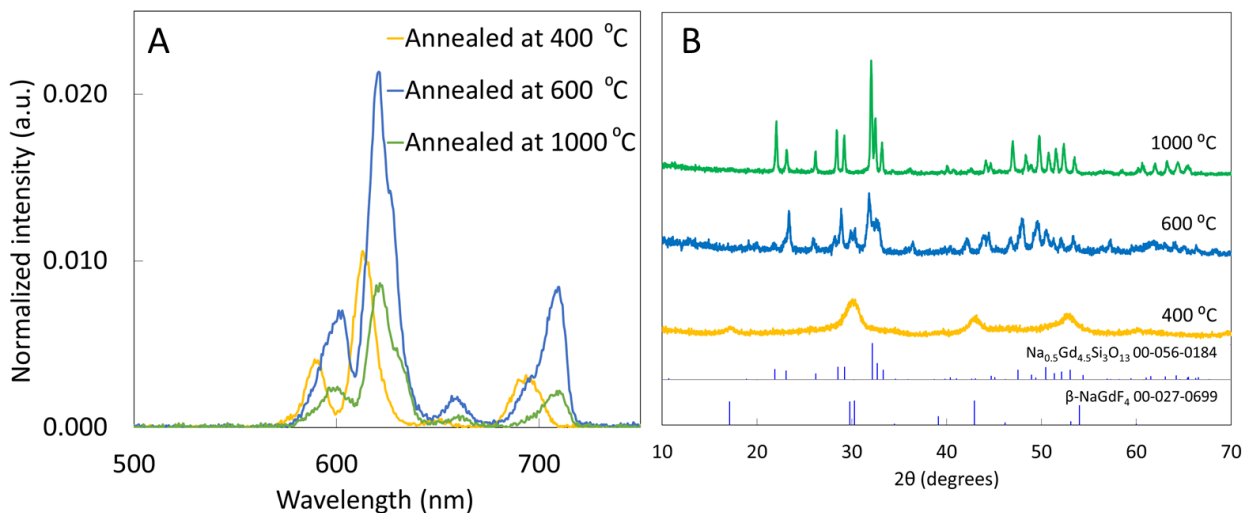


**Figure 9.** (A) XEOL of NaGdF<sub>4</sub>:Eu@SiO<sub>2</sub> annealed at 400 °C, 600 °C and 1000 °C for 6 hrs. (B) Powder XRD pattern of annealed NaGdF<sub>4</sub>:Eu@SiO<sub>2</sub> at 600 °C and 1000 °C compared to PDF cards 00-056-0184 and 00-056-0122.

#### 2.4 Biotin Functionalized NaGdF<sub>4</sub>: Eu@SiO<sub>2</sub>

Functionalizing rare-earth doped nanoparticles are important in *in vivo* labeling and imaging, biological assays and sensor applications with specific targets such as proteins and DNA [12,23,24]. We functionalized NaGdF<sub>4</sub>:Eu@SiO<sub>2</sub> nanoparticles (not annealed) with a mixture of PEG-phosphate and biotin-PEG. The PEG-phosphate was chosen to improve good dispersion of surface-modified nanoparticles in water at physiological pH and high ionic strength (PBS buffer). The biotin-functionalization was demonstrated by attachment to streptavidin-functionalized buoyant silica microbubbles (Figure 10).

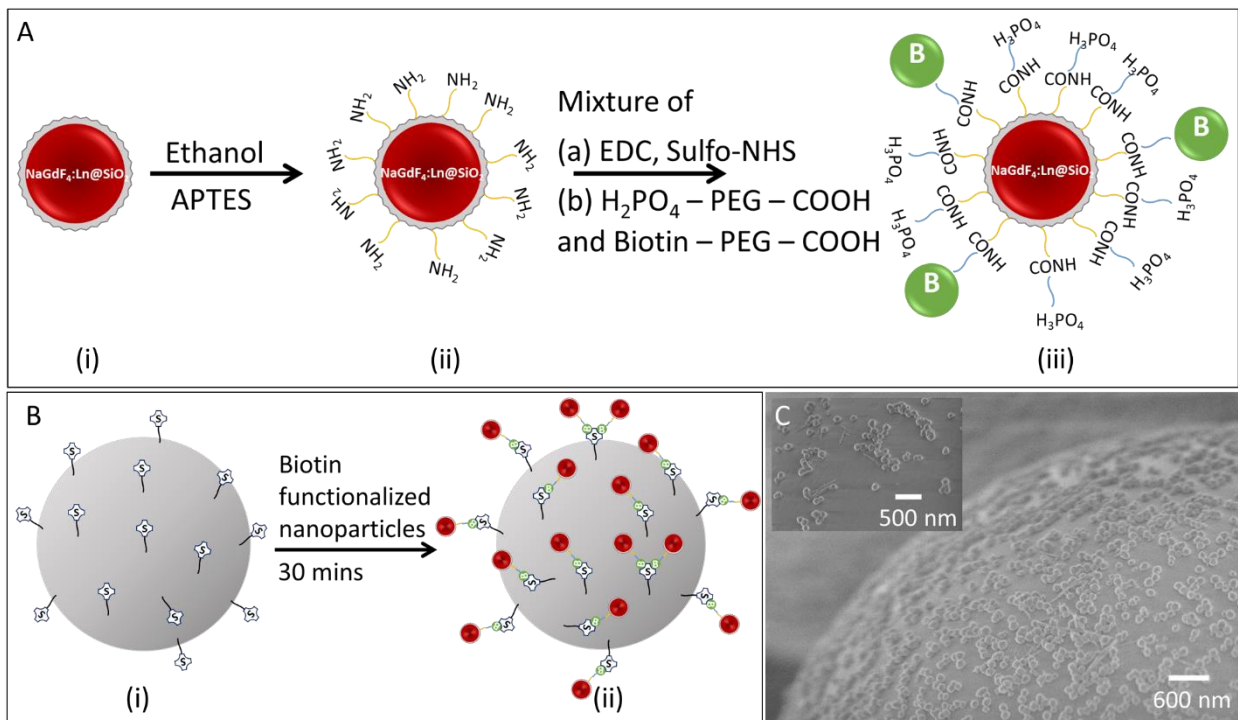


**Figure 10.** Schematic illustration of (A) Silica coated nanoparticles functionalized with biotin (i) Silica-coated NaGdF<sub>4</sub>:Eu nanoparticles, (ii) amine-functionalized nanoparticles, (iii) Biotin-functionalized nanoparticles. Biotin is connected to amine-functionalized nanoparticles via Sulfo-NHS groups, (B) biotin functionalized nanoparticles attach to streptavidin coated silica microbubbles. (i) Streptavidin-coated silica microbubbles, (ii) Biotin-functionalized nanoparticles attached to streptavidin-coated silica microbubbles. (C) SEM image showing biotin-functionalized nanoparticles attached to streptavidin-coated microbubbles.

#### 2.5 X-ray excited optical luminescence spectroscopy and imaging of capillaries filled with NaGdF<sub>4</sub>: Eu through tissue

XEOL spectroscopy and imaging were performed to demonstrate the ability to excite the nanophosphors through tissue and show that the luminescence could be generated in specific regions using a focused X-ray source.

XEOL spectroscopy of colloidal  $\text{NaGdF}_4:\text{Eu}$  nanophosphors in capillaries were measured with and without being sandwiched between two 4 mm porcine tissue. Figure 11. A1 and B1 show a schematic illustration of the experimental setup. The glass slide carrying capillaries (1 mm diameter) filled with a nanoparticle solution (0, 50, 100 mg/mL) is placed on the microscope stage. The light generated in X-ray irradiated nanophosphors was collected through a microscope lens and send to a spectrograph. Spectra generated without tissue (Figure 11. A2) shows intensity higher than capillaries sandwiched between porcine tissues (Figure 11. B2). Also, as the concentration of nanoparticles increase in the capillary intensity increases in both scenarios.

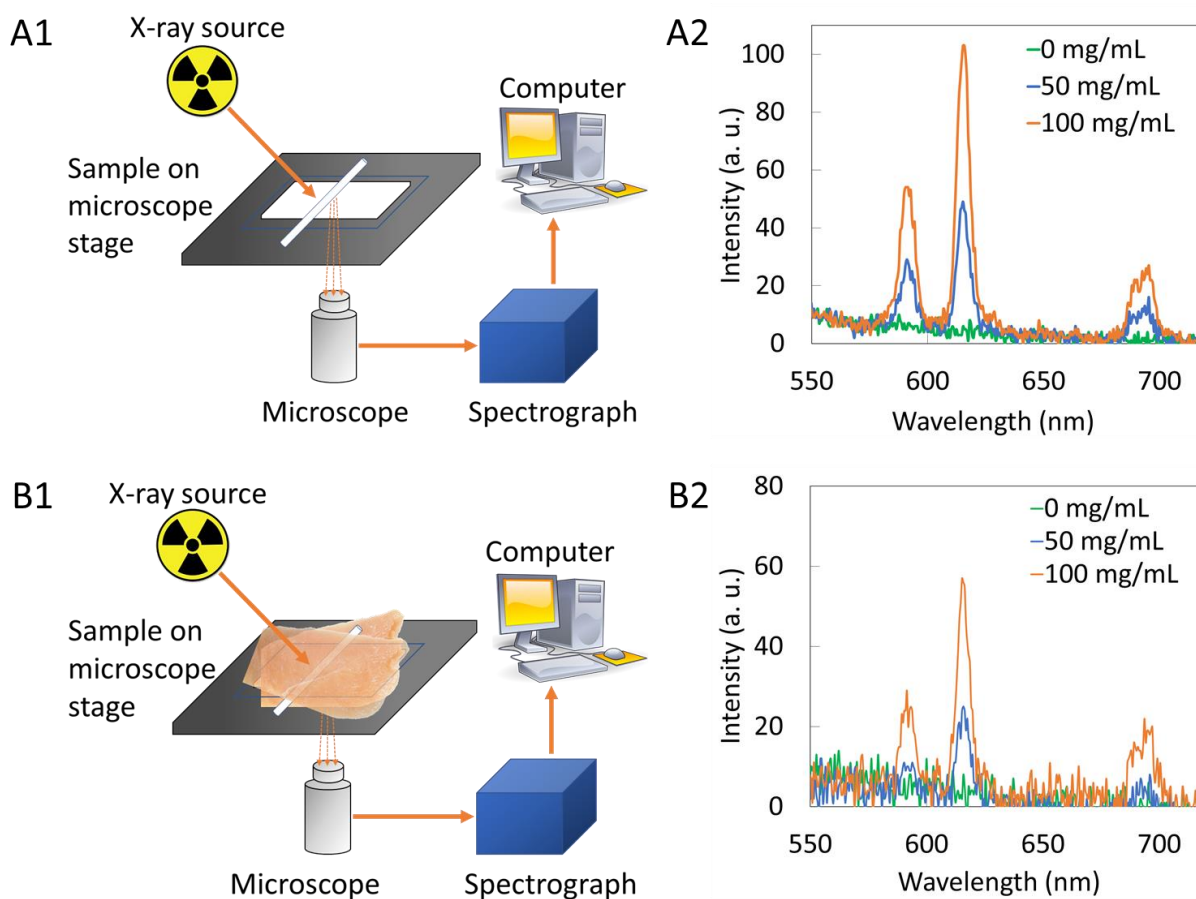


**Figure 11.** Schematic illustration of measuring XEOL of  $\text{NaGdF}_4:\text{Eu}$  filled in capillaries (**A1**) without tissue (**B1**) sandwiched with two 5 mm porcine tissues. XEOL of  $\text{NaGdF}_4:\text{Eu}$  filled in capillaries (**A2**) without tissue (**B2**) sandwiched with two 5 mm porcine tissues. Exposure time was 10 s without tissue and 60 s through tissue.

To demonstrate focused X-ray excited light generation and collection through tissue, we loaded 1 mm diameter glass capillaries with  $\text{NaGdF}_4:\text{Eu}$  nanophosphor dispersions, and placed the capillaries beneath 5 mm porcine tissue for imaging (Figure 12). Three capillaries were used, with  $\text{NaGdF}_4$  concentrations of 0, 50 and 100 mg/mL, respectively. Our 0.75" diameter collection optics and coupled acrylic light guide collected light from a large field of view ( $\sim 1''$ ), but the focused X-ray beam irradiated only a small region ( $\sim 250$   $\mu\text{m}$  spot size). We found a relatively sharp image showing luminescence only from the filled region of the capillaries, and excellent agreement with the X-ray transmission image. The capillary with DI water (0 mg/mL) produced dim luminescence, as glass displays a weak X-ray luminescence signal with a broad spectrum roughly peaking at 430 nm (Supporting info Figure 2). The signal at 50 mg/mL and 100 mg/mL are clearly much larger and increase proportionally to concentration. Importantly, although the signal through tissue was 9.6 times weaker than with no tissue (mainly due to

optical attenuation and partly from X-ray attenuation), the observed spatial resolution was very similar demonstrating local radioluminescence excitation through tissue.

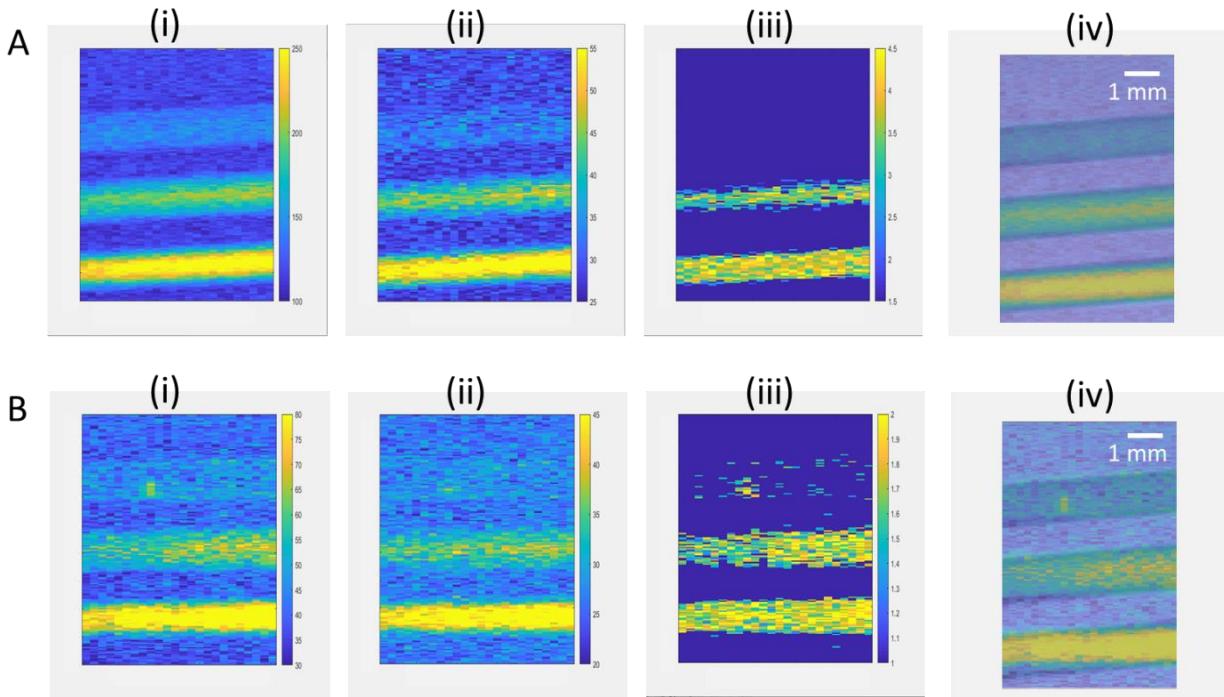


**Figure 12.** XELCI images of NaGdF<sub>4</sub>:Eu dispersion in capillaries (**A**) XELCI images without tissue i) image of 620 nm intensity (counts) vs. position. ii) image of 700 nm intensity (counts) vs. position iii) XELCI ratio image (intensity ratio of 620 nm and 700 nm). (**B**) XELCI images of the same capillaries sandwiched between two 5 mm porcine tissue slices i) 620 nm image ii) 700 nm image iii) XELCI ratio image. iv) Superimposed 620 nm image and X-ray transmittance images. Current was 200  $\mu$ A without tissue and 600  $\mu$ A through tissue. 1 mm scale bar is same for all images.

### 2.6 MR Imaging of NaGdF<sub>4</sub>: Eu and Tb

NaGdF<sub>4</sub>:Eu and Tb may also potentially be T<sub>1</sub> and T<sub>2</sub> weighted MRI contrast agents as previously reported [25,26]. To demonstrate this, varying concentrations of NaGdF<sub>4</sub>: Eu and Tb were prepared in DI water and imaged using a 3T Siemens MAGNATOM Prisma MRI (Figures 13A and 13B). As expected, T<sub>2</sub> weighted images became darker as concentration increased and T<sub>1</sub> weighted images became brighter as concentration increased. MRI imaging would allow for deep tissue imaging, and would be complementary to X-ray luminescence imaging and stimulation.

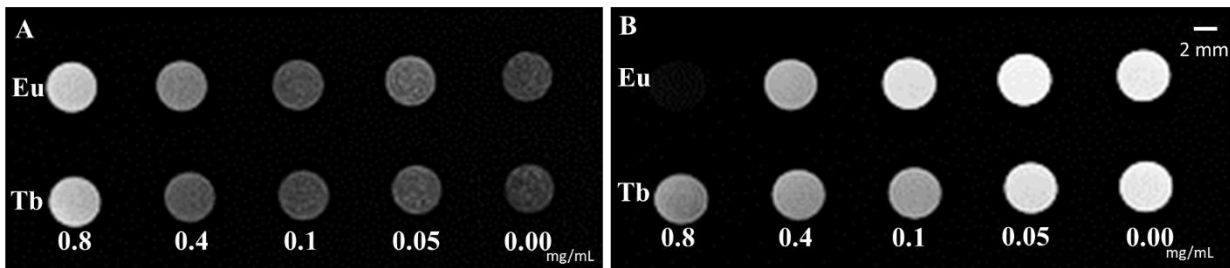


**Figure 13.** Magnetic Resonance Images (MRI) of NaGdF<sub>4</sub>:Eu and NaGdF<sub>4</sub>:Tb nanoparticle suspensions in water. (**A**) T<sub>1</sub> weighted and (**B**) T<sub>2</sub> weighted images with nanoparticle concentration of 0.8, 0.4, 0.1, 0.05 mg/ml, and 0 mg/ml (just water). 2 mm scale bar is same for both T<sub>1</sub> and T<sub>2</sub> weighted images.

### 3. Conclusions

Two simple inorganic synthesis methods were used here to synthesize Eu- and Tb doped NaGdF<sub>4</sub> ~100 nm nanophosphors. The co-precipitation method synthesized spherical-shaped particles, and the hydrothermal method generated irregular particles that yielded higher X-ray excited luminescence intensity. Annealing nanoparticles without silica coating resulted in high luminescence intensity yet aggregated particles. Annealing silica-coated nanoparticles increase the X-ray luminescence intensity. However, at high temperature, it transformed NaGdF<sub>4</sub>:Eu into sodium gadolinium silicate which also shows X-ray luminescence. Then, we functionalized NaGdF<sub>4</sub>:Eu@SiO<sub>2</sub> nanoparticles with biotin and confirmed attaching to streptavidin in vitro. We also selectively excited scintillator nanoparticles using a focused X-ray source to generate light and collect them through the tissue to generate XELCI images and XEOL was measured through tissue. We also showed that the particles could serve as MRI contrast agents. Future work will investigate the spectral shift by changing host materials for multi-analyte imaging through tissue.

### 4. Experimental Section

#### 4.1 Synthesizing NaGdF<sub>4</sub>: Eu and NaGdF<sub>4</sub>: Tb nanoparticles:

##### 4.1.1 Co-precipitate method

NaGdF<sub>4</sub>: Eu and Tb nanoparticles were synthesized by the citrate method with slight modifications [14,27]. Sodium citrate (12 mL of 0.2 M) was added to a clear aqueous solution containing 4 mL of GdNO<sub>3</sub> (0.2 M) and TbNO<sub>3</sub>/ EuNO<sub>3</sub> (X mol%) and stirred vigorously for 30 mins at room temperature. Then, 16 mL of Sodium fluoride (1M) solution was combined with the above mixture and stirred vigorously for another 2 hours which result in a white solution. The synthesized nanoparticles were centrifuged and washed three times before further experiments. (TbNO<sub>3</sub>/ EuNO<sub>3</sub> X mol%= 0.1%, 1%,15% 20%, 100% of Gd<sup>3+</sup> moles)

##### 4.1.2 Hydrothermal method

NaGdF<sub>4</sub>: Eu and Tb nanoparticles were synthesized by the citrate method with slight modifications [14,15,27]. Sodium citrate (12 mL of 0.2 M) was added to a clear aqueous solution containing 4 mL of GdNO<sub>3</sub> (0.2 M) and TbNO<sub>3</sub>/ EuNO<sub>3</sub> (X mol%) and stirred for 30 mins. Then, 16 mL of Sodium fluoride (1M) solution was combined with the above mixture and stirred vigorously for another 15 minutes which result in a white solution. This solution was transferred to a Teflon-lined autoclave and heated at 180 °C for 6 hours. The synthesized nanoparticles were centrifuged and washed three times before further experiments. The synthesized nanoparticles were stored in either DI water or 0.1% citrate solution. (TbNO<sub>3</sub>/ EuNO<sub>3</sub> X mol%= 0.1%, 1%,15% 20%, 100% of Gd<sup>3+</sup> moles).

#### 4.2 Synthesizing NaGdF<sub>4</sub>: Eu and Tb@SiO<sub>2</sub> nanoparticles

Synthesized nanoparticles were coated with silica using Hongyu's method with a slight modification [28,29]. Eu doped and Tb doped NaGdF<sub>4</sub> nanoparticles prepared at room temperature were resuspended in 8 mL of water and combined with 200 mL Ethanol solution containing PVP (1.2 g) and ammonium hydroxide (6 mL). Then, TEOS (160  $\mu$ L) was added after the solution was stirred for 30 mins. The particles were aged another 3 hours before centrifuged and washed using DI water.

#### *4.3 Annealing NaGdF<sub>4</sub>: Eu nanoparticles*

NaGdF<sub>4</sub>:Eu nanoparticles prepared using the co-precipitate method were dried at 80 °C to form a white powder. It was transferred to a crucible and heated (10 °C/min) at 1000 °C for 6 hours in a muffle furnace which results in a solid, aggregated structure. After cooling down to room temperature, it was crushed into a fine powder using mortar and pestle.

NaGdF<sub>4</sub>:Eu@SiO<sub>2</sub> nanoparticles were dried at 80 °C to form a white powder and divide into three portions and transferred to crucibles. The samples were heated at 400 °C, 600 °C and 1000 °C for 6 hours to anneal them.

#### *4.4 Functionalization of NaGdF<sub>4</sub>: Eu@SiO<sub>2</sub> with Biotin*

NaGdF<sub>4</sub>:Eu@SiO<sub>2</sub> nanoparticles were resuspended in ethanol (100 mL) with APTES (300  $\mu$ L) and stirred for 3.5 hr. The amine-functionalized nanoparticles were collected and washed three times using DI water.

98 mL of MES buffer (0.1 M, pH 6.0) was taken in a 500 mL round bottom flask. ~100 mg of water-soluble carbodiimide (EDC) and Sulfo-NHS was added to it and stirred for 15 minutes at room temperature. H<sub>2</sub>PO<sub>4</sub> – PEG – COOH (5000 Da) (500  $\mu$ L, 10 mg/mL) and Biotin–PEG–COOH (1000 Da) (250  $\mu$ L, 10 mg/mL) was added to the above solution and stirred for 1 hour at room temperature to activate COOH groups. Then, the solution pH was adjusted to pH 7.4 using PBS buffer. Previously prepared NH<sub>2</sub> functionalized NaGdF<sub>4</sub>:Eu@SiO<sub>2</sub> nanoparticles were added to the mixture and it could react for 12 hr at room temperature with continuous stirring. Lastly, biotin-conjugated NPs were washed with PBS three times and stored in DI water.

Biotin functionalized aqueous nanoparticles suspension (10 mg/mL, 20  $\mu$ L) was transferred into a centrifuge tube contained PBS (10x, 380  $\mu$ L) solution. Streptavidin-coated microbubbles (100  $\mu$ L) were mixed with the previous solution and vortexed to allow particle adhesion on the surface of the microbubble. After waiting a 10-15 minutes, suspended microbubbles were pipetted out and washed three times with DI water [30,31].

#### *4.5 Imaging capillaries filled with NaGdF<sub>4</sub>: Eu through tissue*

A series of concentration of NaGdF<sub>4</sub>:Eu (100, 50 and 0 mg/ml) was prepared and filled in 1mm (inner diameter) capillaries.

X-ray excited optical luminescence of all the samples in capillaries were measured by irradiating with a Mini-X Ag-target X-ray source at 40 kV and 99  $\mu$ A. Spectral data of capillaries were obtained at 10 s exposure time and capillaries sandwiched in between 4 mm porcine tissue were obtained at 60 s exposure time.

X-ray excited luminescence chemical imaging (XELCI) of these capillaries was done without tissue and with 5mm porcine tissue. The capillaries were scanned with 250  $\mu\text{m}$  step size and 1 mm/sec for a high-resolution scan. For imaging without tissue, the X-ray source was set to 50 kV and 200  $\mu\text{A}$ ; 50 kV and 600  $\mu\text{A}$  was used for imaging with porcine tissue. Data were analyzed and plotted using custom MATLAB scripts.

#### *4.6 Preparing Nanoparticles for MR Imaging of NaGdF<sub>4</sub>: Eu and Tb*

T<sub>1</sub> and T<sub>2</sub> MRI measurements were acquired for the NaGdF<sub>4</sub>: Eu and Tb nanoparticles at a series of concentrations from 0.05 to 0.8 mg/ml by dissolving in DI water. 3T Siemens MAGNATOM Prisma MRI instrument was used to take T<sub>1</sub> and T<sub>2</sub> MRI measurements and images.

#### *Transmission Electron Microscopy*

The synthesized, silica-coated and annealed nanoparticles were deposited on a Formvar/carbon-coated copper grids from a water solution and dried before taking the transmission electron micrographs from Hitachi HT7800 operating at 20- 120 keV and 8  $\mu\text{A}$ .

#### *Powder X-ray Diffraction (XRD)*

The phases of the powders of NaGdF<sub>4</sub>: Eu and nanoparticles and annealed Eu doped NaGdF<sub>4</sub> nanoparticles were characterized by Rigaku Ultima IV powder diffractometer, using Cu K $\alpha$  radiation. Powdered samples were spread on a low background glass slide and data are collected in 0.02-degree increments at a rate of 1 degree per minute from 10 to 70 degrees.

#### *X-ray Excited Optical Luminescence*

X-ray luminescence of all the nanoparticles was measured by irradiating with an X-ray beam. A 96 well plate containing dried and powdered nanoparticles was placed on the stage of an inverted microscope and irradiated with an X-ray beam generated using a Mini-X (Ag) X-ray source (Amptek, Bedford, MA) set at 40 kV and 99  $\mu\text{A}$ . The emission of nanoparticles was collected by 5x objective and focused to a spectrograph (DNS 300, DeltaNu, Laramie, WY, USA), equipped with a cooled CCD camera (iDUS-420BV, Andor, South Windsor, CT, United States)

## **Acknowledgments**

This work was funded by NSF Track II EPSCoR OIA-1632881 for the synthesis by the NIH NIBIB R01EB026646 for the X-ray luminescence imaging, and 5P20GM103444-07 for the electron microscopy. Electron microscopy images were acquired with in the Electron microscope facility, Clemson University, Clemson Research Park, AMRL building. MR images were taken in the Civitan International Neuroimaging Laboratory, University of Alabama at Birmingham.

## Conflicts of Interest

The authors declare no conflict of interest.

## References and Notes

1. Rodnyi, P.A. *Physical Processes in Inorganic Scintillators*; CRC Press, 1997; ISBN 978-0-8493-3788-8.
2. Lecoq, P. Scintillation Detectors for Charged Particles and Photons. In *Detectors for Particles and Radiation. Part 1: Principles and Methods*; Fabjan, C.W., Schopper, H., Eds.; Landolt-Börnstein - Group I Elementary Particles, Nuclei and Atoms; Springer Berlin Heidelberg: Berlin, Heidelberg, 2011; Vol. 21B1, pp. 45–71 ISBN 978-3-642-03605-7.
3. Birowosuto, M.D.; Dorenbos, P.; van Eijk, C.W.E.; Krämer, K.W.; Güdel, H.U. High-light-output scintillator for photodiode readout: Lu<sub>3</sub>:Ce<sup>3+</sup>. *Journal of Applied Physics* **2006**, *99*, 123520, doi:10.1063/1.2207689.
4. *Radiation detectors for medical applications*; Tavernier, S., North Atlantic Treaty Organization, Eds.; NATO security through science series; Springer: Dordrecht, 2006; ISBN 978-1-4020-5091-6.
5. Chen, H.; Moore, T.; Qi, B.; Colvin, D.C.; Jelen, E.K.; Hitchcock, D.A.; He, J.; Mefford, O.T.; Gore, J.C.; Alexis, F.; et al. Monitoring pH-triggered drug release from radioluminescent nanocapsules with X-ray excited optical luminescence. *ACS Nano* **2013**, *7*, 1178–1187, doi:10.1021/nn304369m.
6. Chen, H.; Qi, B.; Moore, T.; Colvin, D.C.; Crawford, T.; Gore, J.C.; Alexis, F.; Mefford, O.T.; Anker, J.N. Synthesis of brightly PEGylated luminescent magnetic upconversion nanophosphors for deep tissue and dual MRI imaging. *Small* **2014**, *10*, 160–168, doi:10.1002/smll.201300828.
7. Development of NIR-Emitting Scintillators Based on Rare-Earth-Doped Garnet Crystals – Part 1. *Sensors and Materials* **2017**, 1407, doi:10.18494/SAM.2017.1620.
8. Zhou, J.; Liu, Z.; Li, F. Upconversion nanophosphors for small-animal imaging. *Chem. Soc. Rev.* **2012**, *41*, 1323–1349, doi:10.1039/C1CS15187H.
9. Pratz, G.; Carpenter, C.M.; Sun, C.; Xing, L. X-Ray Luminescence Computed Tomography via Selective Excitation: A Feasibility Study. *IEEE Transactions on Medical Imaging* **2010**, *29*, 1992–1999, doi:10.1109/TMI.2010.2055883.
10. Chen, H.; Wang, F.; Moore, T.L.; Qi, B.; Sulejmanovic, D.; Hwu, S.-J.; Mefford, O.T.; Alexis, F.; Anker, J.N. Bright X-ray and up-conversion nanophosphors annealed using encapsulated sintering agents for bioimaging applications. *J. Mater. Chem. B* **2017**, *5*, 5412–5424, doi:10.1039/C7TB01289F.
11. Lun, M.C.; Cong, W.; Arifuzzaman, M.; Ranasinghe, M.; Bhattacharya, S.; Anker, J.; Wang, G.; Li, C. X-ray luminescence imaging for small animals. In *Proceedings of the Optics and Ionizing Radiation*; International Society for Optics and Photonics, 2020; Vol. 11224, p. 112240F.
12. Wang, F.; Banerjee, D.; Liu, Y.; Chen, X.; Liu, X. Upconversion nanoparticles in biological labeling, imaging, and therapy. *Analyst* **2010**, *135*, 1839–1854, doi:10.1039/C0AN00144A.
13. Berry, R.; Getzin, M.; Gjestebj, L.; Wang, G. X-Optogenetics and U-Optogenetics: Feasibility and Possibilities. *Photonics* **2015**, *2*, 23–39, doi:10.3390/photonics2010023.
14. Sudheendra, L.; Das, G.K.; Li, C.; Stark, D.; Cena, J.; Cherry, S.R.; Kennedy, I.M. NaGdF<sub>4</sub>: Eu<sup>3+</sup> nanoparticles for enhanced X-ray excited optical imaging. *Chem. Mater.* **2014**, *26*, 1881–1888, doi:10.1021/cm404044n.
15. F, H.; P, Y.; D, W.; N, N.; S, G.; X, L. Self-assembled β-NaGdF<sub>4</sub> microcrystals: hydrothermal synthesis, morphology evolution, and luminescence properties. *Inorg Chem* **2011**, *50*, 4116–4124, doi:10.1021/ic200155q.
16. Ren, Y.; Winter, H.; Rosch, J.G.; Jung, K.; Duross, A.N.; Landry, M.R.; Pratz, G.; Sun, C. PEGylated β-NaGdF<sub>4</sub>/Tb@CaF<sub>2</sub> Core/Shell Nanophosphors for Enhanced Radioluminescence and

- Folate Receptor Targeting. *ACS Appl. Nano Mater.* **2019**, *2*, 3718–3727, doi:10.1021/acsanm.9b00629.
17. Yanagida, T. Study of rare-earth-doped scintillators. *Optical Materials* **2013**, *35*, 1987–1992, doi:10.1016/j.optmat.2012.11.002.
  18. Guan, H.; Liu, G.; Wang, J.; Dong, X.; Yu, W. Multicolor tunable luminescence and paramagnetic properties of NaGdF<sub>4</sub>:Tb<sup>3+</sup>/Sm<sup>3+</sup> multifunctional nanomaterials. *Dalton Trans.* **2014**, *43*, 10801–10808, doi:10.1039/C4DT00158C.
  19. Sedlmeier, A.; Gorris, H.H. Surface modification and characterization of photon-upconverting nanoparticles for bioanalytical applications. *Chem. Soc. Rev.* **2015**, *44*, 1526–1560, doi:10.1039/C4CS00186A.
  20. Li, X.; Xue, Z.; Jiang, M.; Li, Y.; Zeng, S.; Liu, H. Soft X-ray activated NaYF<sub>4</sub>:Gd/Tb scintillating nanorods for in vivo dual-modal X-ray/X-ray-induced optical bioimaging. *Nanoscale* **2017**, *10*, 342–350, doi:10.1039/C7NR02926H.
  21. Sagaydachnaya, E.A.; Kochubey, V.I.; Konyukhova, J.G. Influence of annealing temperature on the upconversion luminescence properties of NaYF<sub>4</sub>:Er,Yb@SiO<sub>2</sub> particles. *J. Phys.: Conf. Ser.* **2017**, *917*, 032006, doi:10.1088/1742-6596/917/3/032006.
  22. Li, Y.; Li, Y.; Wang, R.; Xu, Y.; Zheng, W. Enhancing upconversion luminescence by annealing processes and the high-temperature sensing of ZnO:Yb/Tm nanoparticles. *New J. Chem.* **2017**, *41*, 7116–7122, doi:10.1039/C7NJ01358B.
  23. Wang, M.; Abbineni, G.; Clevenger, A.; Mao, C.; Xu, S. Upconversion nanoparticles: synthesis, surface modification and biological applications. *Nanomedicine: Nanotechnology, Biology and Medicine* **7**, 710–729.
  24. Bouzigues, C.; Gacoin, T.; Alexandrou, A. Biological Applications of Rare-Earth Based Nanoparticles. *ACS Nano* **2011**, *5*, 8488–8505, doi:10.1021/nn202378b.
  25. Lu, Z. Size-tunable NaGdF<sub>4</sub> nanoparticles as T2 contrast agents for high-field magnetic resonance imaging. *RSC Advances* **2017**, *7*.
  26. Lu, W.; Liao, Y.; Jiang, C.; Wang, R.; Shan, X.; Chen, Q.; Sun, G.; Liu, J. Polydopamine-coated NaGdF<sub>4</sub>:Dy for T<sub>1</sub>/T<sub>2</sub>-weighted MRI/CT multimodal imaging-guided photothermal therapy. *New J. Chem.* **2019**, *43*, 7371–7378, doi:10.1039/C9NJ00561G.
  27. Li, J.; Hao, Z.; Zhang, X.; Luo, Y.; Zhao, J.; Lü, S.; Cao, J.; Zhang, J. Hydrothermal synthesis and upconversion luminescence properties of β-NaGdF<sub>4</sub>:Yb<sup>3+</sup>/Tm<sup>3+</sup> and β-NaGdF<sub>4</sub>:Yb<sup>3+</sup>/Ho<sup>3+</sup> submicron crystals with regular morphologies. *J Colloid Interface Sci* **2013**, *392*, 206–212, doi:10.1016/j.jcis.2012.09.076.
  28. Chen, H.; Qi, B.; Moore, T.; Wang, F.; Colvin, D.C.; Sanjeewa, L.D.; Gore, J.C.; Hwu, S.-J.; Mefford, O.T.; Alexis, F.; et al. Multifunctional yolk-in-shell nanoparticles for pH-triggered drug release and imaging. *Small* **2014**, *10*, 3364–3370, doi:10.1002/sml.201303769.
  29. Chen, H.; Sulejmanovic, D.; Moore, T.; Colvin, D.C.; Qi, B.; Mefford, O.T.; Gore, J.C.; Alexis, F.; Hwu, S.-J.; Anker, J.N. Iron-Loaded Magnetic Nanocapsules for pH-Triggered Drug Release and MRI Imaging. *Chem Mater* **2014**, *26*, 2105–2112, doi:10.1021/cm404168a.
  30. Chen, X.; Liu, Y.; Tu, D. Surface Modification Chemistry of Lanthanide-Doped Nanoparticles. In *Lanthanide-Doped Luminescent Nanomaterials; Nanomedicine and Nanotoxicology*; Springer Berlin Heidelberg: Berlin, Heidelberg, 2014; pp. 59–74 ISBN 978-3-642-40363-7.
  31. Asakura, R.; Isobe, T.; Kurokawa, K.; Aizawa, H.; Ohkubo, M. Tagging of avidin immobilized beads with biotinylated YAG:Ce<sup>3+</sup> nanocrystal phosphor. *Anal Bioanal Chem* **2006**, *386*, 1641–1647, doi:10.1007/s00216-006-0814-6.